ABSTRACT

Kenneth Kenji Yamamoto
Creating Block Copolymers via Surface-Initiated Ring-Opening Metathesis Polymerization
Under the Direction of Jason Locklin, Ph.D.

A method for the formation of norbornene (Nb) and furan-maleic anhydride (FMA) homopolymers, as well as Nb-FMA and FMA-Nb block copolymers grafted from oxide surfaces was devised using surface-initiated ring-opening metathesis polymerization (SI-ROMP) from a 7-octenyltrichlorosilane (7-OCT) self-assembled monolayers (SAMs) with first generation Grubbs catalyst. Polymer film growth, as monitored by ellipsometry and visualized by atomic force microscopy (AFM), is strongly influenced by monomer structure and concentration, as well as reaction time and temperature. End-functionalization of growing polymer chains occurs through cross-metathesis vinyl containing moieties was demonstrated and confirmed using static water contact angle measurements. Other than introducing chemical functionality into polymeric coating through monomer design, end-functionalization of grafted polymer chains provides a route to tailor functionality into polymer coatings at lower concentrations and is another technique useful for altering surface energy and wettability.

INDEX WORDS: polymer brush, self-assembled monolayer, surface-initiated ring-opening metathesis polymerization, block copolymer, Grubbs catalyst, end-functionalization, cross-metathesis, ellipsometry, contact angle, surface energy, wettability

CREATING BLOCK COPOLYMERS VIA SURFACE-INITIATED RING-OPENING METATHESIS POLYMERIZATION

by

KENNETH KENJI YAMAMOTO

A Thesis Submitted to the Honors Council of The University of Georgia in Partial Fulfillment of the Requirements for the Degrees

BACHELOR OF SCIENCE

in CHEMISTRY

and

BACHELOR OF SCIENCE

in MATHEMATICS

and

BACHELOR OF ARTS

in GERMAN

with HIGH HONORS

Athens, Georgia

2009

CREATING BLOCK COPOLYMERS VIA SURFACE-INITIATED RING-OPENING

METATHESIS POLYMERIZATION

by

KENNETH KENJI YAMAMOTO

Approved:

Dr. Jason Locklin 5/10/2009

_____ _____

Dr. Jason Locklin Date
Faculty Research Mentor

Approved:

Dr. Timothy Dore 5/7/2009

_____ _____

Dr. Timothy Dore Date
Reader

Approved:

Dr. David S. Williams 5/8/2009

_____ _____

Dr. David S. Williams Date
Director, Honors Program, Foundation Fellows and
Center for Undergraduate Research Opportunities

Approved:

Dr. Pamela B. Kleiber 5/8/2009

_____ _____

Dr. Pamela B. Kleiber Date
Associate Director, Honors Program and
Center for Undergraduate Research Opportunities

DEDICATION

To my parents

ACKNOWLEDGEMENTS

First and foremost I thank Dr. Jason Locklin for his mentorship to me. No other person could bring as much impassioned enthusiasm to research than him. I count myself very lucky to have had him as my undergraduate research mentor. To him I owe so much.

I also thank members of the Locklin Group for all their help. Satya Samanta, Nick Marshall, Gareth Sheppard, Sara Orski, Kristen Fries, and Kyle Sontag, you have all tolerated much from me, especially my accident-prone tendencies. It has been fun.

I am grateful also for every teacher who have been a part of my education at The University of Georgia, including Dr. Timothy Dore, who never failed to challenge me throughout three semesters of organic chemistry and then also in the reading of this thesis.

Wherever life may take me, I will never forget all of you who have made me who I am today. Thank you all very much!

TABLE OF CONTENTS

LIST OF TABLES

Page

LIST OF FIGURES

Page

LIST OF EQUATIONS

Page

LIST OF ABBREVIATIONS

Nb = Norbornene

FMA = Furan-Maleic Anhydride

SI-ROMP = Surface-Initiated Ring-Opening Metathesis Polymerization

7-OCT = 7-Cctenyltrichlorosilane

SAM = Self-Assembled Monolayer

AFM = Atomic Force Microscopy

IUPAC = International Union of Pure and Applied Chemistry

ROMP = Ring-Opening Metathesis Polymerization

ATRP = Atom-Transfer Radical Polymerization

SPM = Scanning Probe Microscopy

PSD = Position Sensitive Detector

CCD = Charge-Coupled Device

SiO_x/Si = Silicon-Oxide/Silicon

DCM = Dichloromethane

THF = Tetrahydrofuran

HCl = Hydrochloric Acid

μCP = Microcontact Printing

CFL = Capillary Force Lithography

CHAPTER 1
INTRODUCTION

Development of functional surfaces with controlled properties such as wetting, adhesion, lubrication, corrosion, and friction is fundamental in technological applications, including microfluidic devices,[1] controllable drug delivery,[2] optical data storage,[3-5] photocontrol of liquid motion,[6-8] self-cleaning surfaces,[9] and biological and chemical sensors.[10] Novel and sophisticated polymer brush constructions on surfaces have been investigated both to create surfaces with desired characteristics, as well as to provide unique opportunities to increase basic understanding of self-organization, structure/property relationships, and new chemical phenomena at gas/solid and liquid/solid interfaces. With its broad applicative potential and scientific relevance, development of functional surfaces have stimulated much interdisciplinary research, merging research efforts of many fields including chemistry, physics, biology, materials and bioengineering, computer science, and medicine.

Surface-initiated polymerizations offer a large array of options for tuning surface properties of materials. By adjusting various factors, including the degree of polymerization (molecular weight), grafting density, and chemical composition, polymer brushes present` an unprecedented means of controlling physical and chemical characteristics of various interfaces used for engineering surfaces. While the synthetic possibilities are vast, fundamental structure-property relationships aimed at understanding the interaction and effect of these parameters on constructing functional surfaces is relatively sparse. In an effort to understand the structure/property relationships of various polymer brush assemblies, the work in this thesis is

aimed at investigating block copolymer systems with layers characterized by greatly differing polarity and thus hydrophilicity. Layers with greatly differing chemical characteristics grafted in highly close proximities present new physical and chemical interactions that can be used to confer new insight into structure/property characteristics of polymer brushes with various surface modifications.

Background

Basic Principles

Polymer Brushes

Though their structures may be highly complex, polymer brushes are essentially polymer chains end-tethered to a surface, whose conformational structure depends on many factors, including degree of polymerization (molecular weight), grafting density, interactions between tethered polymer chains, between tethered chains and the substrate, and between tethered chains and the surrounding chemical environment such as the solvent. As grafting density is increased, surface-bound polymer chains stretch away from the substrate due to the volume-excluded effect, where polymer chains grafted from surfaces in high density extend outwards from the surface since spaces adjacent to polymer chains are occupied by other chains and no two chains can occupy the same space (**Figure 1.1**). By investigating synthetic strategies to control polymer architecture, functionality, and nanostructure, as well as understanding the correlation between polymer chemistries and material characteristics, it is possible to precisely manufacture materials with new characteristics and functionalities. Functional or stimuli-responsive polymer brushes are developed to be responsive to regulation, adjustment, and switching of interaction forces between the brush and its environment, which may consist of liquid, vapor, solid, another polymer brush, particles, or other materials.

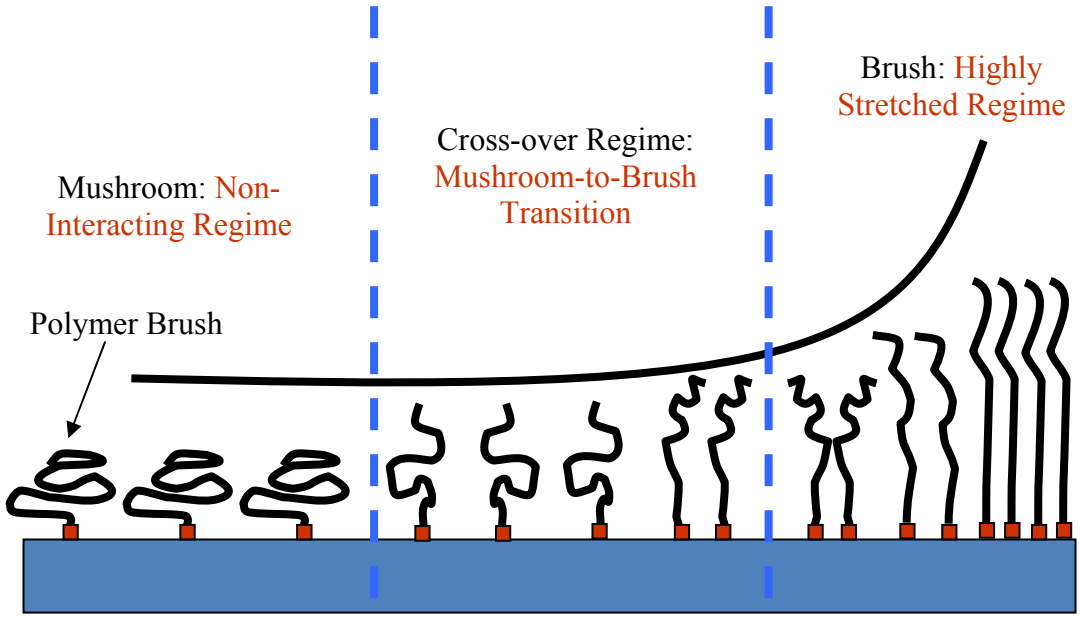

Figure 1.1: Polymer Brush Conformation Affected by Grafting Density.

While prefabricated polymer chains with end group or side chain functionality can be covalently attached *to the surface* in low densities to create non-interacting "polymer mushrooms" in the "grafting-to" approach, the "grafting-from" approach polymerizes chains *from the surface* at high density. Polymer brushes are grafted from surfaces via surface-initiated polymerization techniques, including ring-opening metathesis polymerization (ROMP), atom-transfer radical polymerization (ATRP), and various types of free radical polymerization, which all use surface-immobilized initiators for *in situ* generation of grafted polymers. At high grafting densities, polymer brushes are physically forced to assume a highly stretched regime, where chains are extended from the surface by the volume-excluded effect, which is otherwise entropically impossible. Synthesis of polymer chains extending from the surface in entropically disfavored "brush" conformations result in chemical systems with high potential energies, which

may also be increased by repulsive forces between polymer chains grafted in highly close proximities.

Creation of functional surfaces seek to utilize the high potential energies intrinsic to various polymer brush constructions as a driving force to polymer chain reorganization, which direct the responsiveness of polymer thin films to various external stimuli, including solvent polarity, changes in temperature, pH, or ionic strength. Block-copolymer brushes that contain two responsive blocks enhance the number of possible changes that polymer films may undergo in response to multiple environmental triggers.

Chemical functionalization of polymer chains offers a relatively simple method in synthesizing functional polymer brushes. Dense arrays of end-tethered polymer chains could be synthesized via surface-initiated polymerizations of monomer that has been chemically functionalized with desired moieties. By grafting polymer chains with chemical functionalities in this way, it is possible to covalently attach chemical functionalities at the surface at high concentrations, which amplifies the effect and responsiveness of polymer brushes to external stimuli.

Self-Assembled Monolayers (SAMs)

To create densely packed polymer brushes using the "grafting-from" approach, surface-initiated polymerizations are performed from self-assembled monolayers (SAMs). A SAM is a single, organized, closely packed layer of long-chain amphiphilic molecules that contains specific functionality, the "head group," that can covalently bind to the surface while the other end, the "tail groups," extend away from the substrate and can carry other chemical functionality (**Figure 1.2**). Typically, chemisorption of hydrophilic "head groups" onto a substrate from either the vapor or liquid phase is followed by a two-dimensional organization of hydrophobic "tail

groups."[11,12] While the "head-group" stabilizes the molecule onto the substrate, the alkyl spacer provides a well-defined thickness, acts as a physical barrier, and alters electronic conductivity and local optical properties. The interface created by the "tail groups" determines the surface properties and presents chemical functional groups. Monolayers pack tightly to increase Van der Waals interactions, thereby reducing the system's free energy. [13]

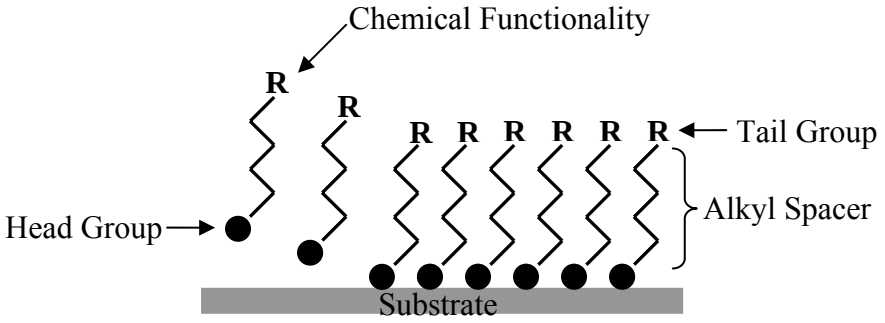

Figure 1.2: Self-Assembled Monolayer (SAM).

Olefin Metathesis and Ring-Opening Metathesis Polymerization (ROMP)

Compared to various other surface-initiated polymerization techniques, ring-opening metathesis polymerization (ROMP) has been attractive because of rapid polymerization and mild reaction conditions, which are driven by relief of ring strain in the monomer. ROMP is a type of olefin metathesis or transalkylidenation reaction, a class of organic reactions that result in redistribution of alkene fragments by the scission of carbon-carbon double bonds in olefins via carbene (alkylidene) exchange by the mechanism shown in **Figure 1.3**.[14,15] The metathesis mechanism begins with the [2+2] cycloaddition of an alkene double bond to a transition metal alkylidene to form a metallocyclobutane intermediate, which has a high activation energy since the direct [2+2] cycloaddition of two alkenes is symmetry forbidden. [2+2] cycloreversion of the

metallocyclobutane intermediate then produces the original species or a new alkene and metal alkylidene. The metathesis reaction resumes in a catalytic cycle as the new metal alkylidene reacts with another substrate alkene to form another metallocyclobutane intermediate. Since these reactions are reversible, olefin metathesis reactions are driven by a thermodynamic imperative, equilibrating to yield more thermodynamically stable products.

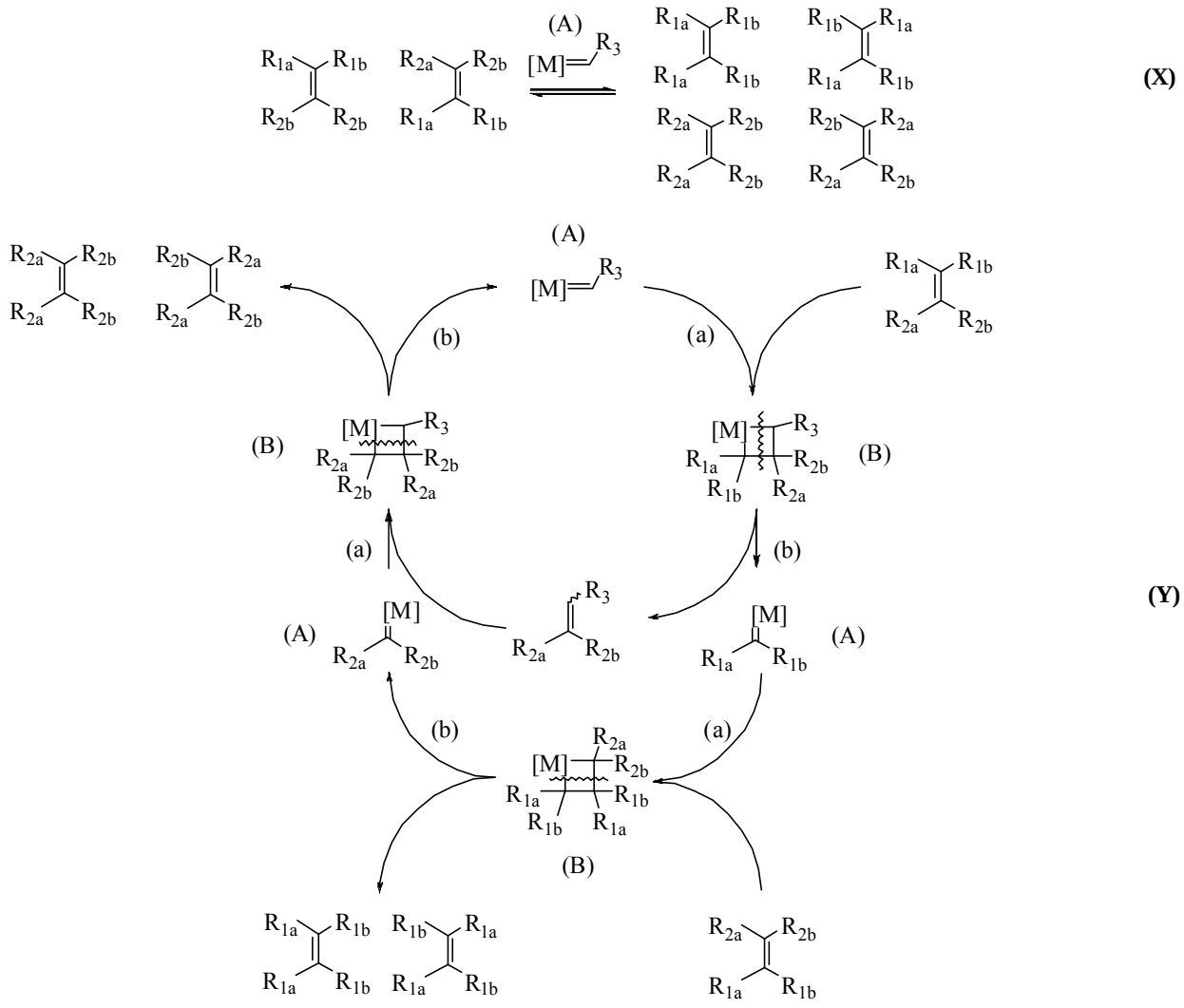

Figure 1.3: Olefin Metathesis Mechanism. The catalytic cycle only shows the forward reaction. (X) = olefin metathesis reaction; (Y) = Chauvin catalytic cycle for olefin metathesis; (A) = transition metal alkylidene; (B) = metallocyclobutane intermediate; (a) = [2+2] cycloaddition; (b) = [2+2] cycloreversion.

ROMP occurs specifically when the olefins are strained cyclic alkenes via the polymerization mechanism shown in **Figure 1.4**. A wide range of transition metal catalysts that initiate ROMP have been discovered, which are tailored to specific monomer characteristics such as the interactions of its substituents.[16] The type of catalyst, monomer identity and concentration, and temperature all influence polymerization kinetics.[17] Since the equilibrium of the catalytic cycle for ROMP is driven towards the ring-opened product via relief of ring-strain in polymerizing strained cyclic alkenes, monomers that undergo ROMP are limited to cyclic alkenes that are lower than five-membered.[18] Bicyclic rings, such as the norbornene (Nb)-based monomers used in this experiment, and tricyclic rings are most effective for ROMP.[19] For ROMP and most other olefin metathesis reactions, First Generation Grubbs Catalyst (IUPAC name: benzylidene-bis(tricyclohexylphosphine)dichlororuthenium) is preferred for its stability in air and compatibility with a large variety of functional groups.[20]

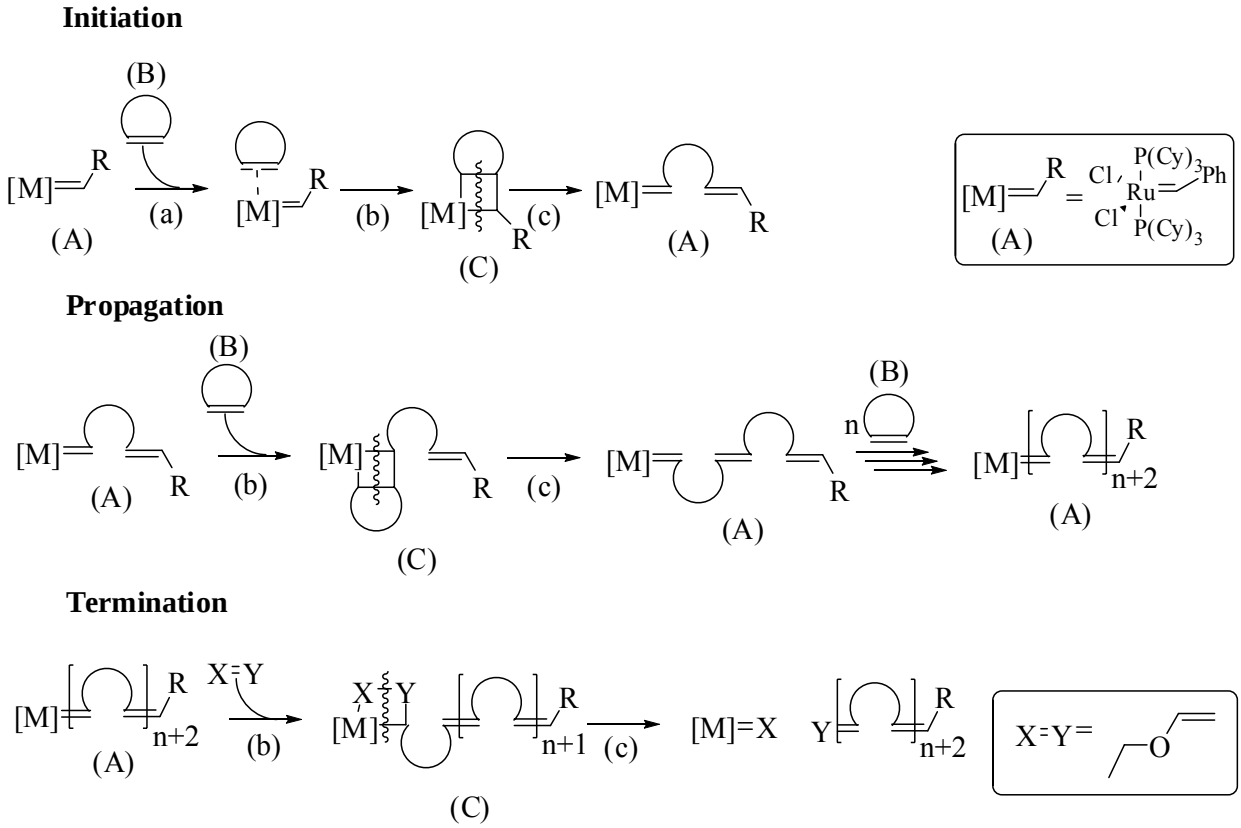

Figure 1.4: Ring-Opening Metathesis Polymerization (ROMP) Mechanism. (A) = transition metal alkylidene (First Generation Grubbs Catalyst); (B) = strained cyclic alkene monomer; (C) = metallocyclobutane intermediate; (a) = coordination; (b) = [2+2] cycloaddition; (c) = [2+2] cycloreversion.

Thin Film Characterization Techniques

Ellipsometry

Ellipsometry, an optical technique that measures change in polarization of light upon reflection or transmission, is a non-destructive and contactless method of characterizing thickness of single or multiple layers on reflective substrates ranging from a few angstroms to several micrometers with excellent accuracy. Standard ellipsometric modeling techniques are only effective for thin film samples consisting of a small number of distinct, optically homogeneous and isotropic layers. However, more advanced procedures, including generalized

and spectroscopic rather than standard, single-wavelength approaches, could be applied for situations that violate these conditions to yield useful data.

In the experimental setup, electromagnetic radiation is first linearly polarized by a polarizer and passed through a compensator, such as a quarter wave plate, before reflection upon the thin film substrate (**Figure 1.5**). The linearly polarized light is reflected from the surface and is elliptically polarized before passing through an optional compensator or phase-modulator and a second polarizer, called the analyzer that nullifies the signal before reaching the detector. Angles of incidence and reflection were measured by mounting the laser and detector on a goniometer, an instrument that allows objects to be rotated to precise angular positions.

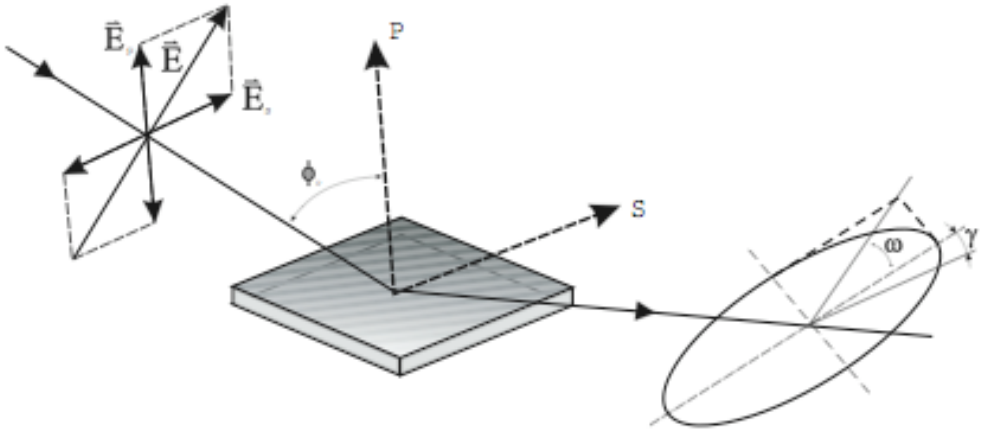

Figure 1.5: Experimental Setup of Ellipsometry.

In standard ellipsometry, where *s*- and *p*-polarized light are not interconverted, two of the four Stokes parameters are determined, which are denoted by Δ and Ψ. Where the incident and reflected beams span the plane of incidence, *s*-polarized light is the component of the light that is polarized perpendicular and *p*-polarized light is the component that is polarized parallel to the

plane of incidence. This is accomplished by first measuring the amplitudes of the *s*- and *p*-polarized components of light reflected off the thin film sample and then normalizing amplitude measurements to their respective initial values in the incident beam. The relationship of normalized *s*- and *p*-polarized components of reflected light and the two Stokes parameters, Δ and Ψ, are described by the following fundamental equation of ellipsometry:

$$\rho = \frac{r_p}{r_s} = \tan(\Psi)e^{i\Delta} \quad \textbf{(Equation 1.1)}$$

where r_p = amplitude of the *p*-polarized component of reflected light, r_s = amplitude of the *s*-polarized component of reflected light, $\tan(\Psi) = \frac{|r_p|}{|r_s|}$ = amplitude ratio of *p*- and *s*-polarized light upon reflection, and $\Delta = \delta_1 - \delta_2$ = phase difference (where δ_1 = phase before reflection and δ_2 = phase after reflection)

Since direct inversion of Δ and Ψ into optical constants and thickness parameters for the sample is only possible in very simple cases of isotropic, homogenous, and infinitely thick films, a model analysis is typically performed. In the model analysis, a layer model is established with known optical constants, including both the real and imaginary parts of refractive indices, and thickness parameters of all individual layers of the thin film sample in the correct layer sequence. An iterative, least-squares minimization procedure then varies unknown optical constants and/or thickness parameters to calculate Δ and Ψ using the following Fresnel equations that best match experimental data:

$$r_s = \left[\frac{\sin(\theta_t - \theta_i)}{\sin(\theta_t + \theta_i)}\right]^2 = \left[\frac{n_1\cos(\theta_i) - n_2\cos(\theta_t)}{n_1\cos(\theta_i) + n_2\cos(\theta_t)}\right]^2 = \left[\frac{n_1\cos(\theta_i) - n_2\sqrt{1-\left(\frac{n_1}{n_2}\sin\theta_i\right)^2}}{n_1\cos(\theta_i) + n_2\sqrt{1-\left(\frac{n_1}{n_2}\sin\theta_i\right)^2}}\right]^2$$ (**Equation 1.2, 1.3**)

$$r_p = \left[\frac{\tan(\theta_t - \theta_i)}{\tan(\theta_t + \theta_i)}\right]^2 = \left[\frac{n_1\cos(\theta_t) - n_2\cos(\theta_i)}{n_1\cos(\theta_t) + n_2\cos(\theta_i)}\right]^2 = \left[\frac{n_1\sqrt{1-\left(\frac{n_1}{n_2}\sin\theta_i\right)^2} - n_2\cos(\theta_i)}{n_1\sqrt{1-\left(\frac{n_1}{n_2}\sin\theta_i\right)^2} + n_2\cos(\theta_i)}\right]^2$$

where r_p = amplitude of the *p*-polarized component of reflected light, r_s = amplitude of the *s*-polarized component of reflected light, θ_i = angle of incident ray to the normal of substrate interface, θ_t = angle of refracted ray to the normal of substrate interface, n_1 = refractive index of the medium of incident ray, n_2 = refractive index of the sample layer

By measuring a ratio rather than absolute values, ellipsometry is relatively insensitive to light scattering, fluctuations, or absorptions due to light source instabilities and/or the atmosphere and requires no calibration with standard samples or reference beams. Also, since it detects phase and polarization state changes, ellipsometry is not diffraction-limited like many other optical techniques. With these aforementioned characteristics, ellipsometric characterization is robust, accurate, and reproducible with angstrom resolution.

Atomic Force Microscopy (AFM)

By monitoring deflections of a microscale cantilever with a sharp tip probe scanning a surface, atomic force microscopy (AFM) is a type of scanning probe microscopy (SPM), where topographic images of sample surfaces are obtained by mechanically probing specimens in a raster scan and recording probe-surface interaction as a function of position.

In the experimental apparatus, a sharp tip probe typically made of silicon or silicon nitride with a radius of curvature of about 10 nanometers at the end of a microscale cantiliever is scanned line by line across a specimen surface. Within sufficiently close proximities to the

sample surface, various attractive and repulsive forces between the tip and the sample lead to deflections of the scanning cantilever according to Hooke's law:

$$F = kx \quad \textbf{(Equation 1.4)}$$

where F = restoring force of the cantilever, x = distance the cantilever has been stretched or compressed away from the equilibrium position, and k = a force constant

Interactive forces that are measured include mechanical contact force, Van der Waals or dipole-dipole forces, capillary forces, atomic bonding, electrostatic forces, magnetic forces, Casimir forces, and solvation forces, including those of dissolution in liquids and single molecule stretching.[21] Cantilever deflection is detected via reflection of laser light from a solid state diode off of the top of the cantilever into a position sensitive detector (PSD) with two closely spaced photodiodes connected to a differential amplifier that collects output signals. Since angular displacement of the deflecting cantilever results in one photodiode collecting more light than the other, an output signal is produced, where the difference between the photodiode signals in the two photodiodes normalized by their sum is proportional to the deflection of the cantilever. Changes in reflected laser beam angles are amplified with a long beam path of several centimeters, allowing for detection of cantilever deflections even under 1 angstrom, more than a thousand times better than the optical diffraction limit.

To avoid probe tip collision with sample surface, probing on specimens are done at constant force rather than constant height. In various setups using piezoelectric actuators that execute precise, accurate motions at the atomic level upon electric command, a feedback mechanism adjusts tip-to-sample distances to maintain constant force between the tip and the sample. For example, the sample may be mounted on a piezoelectric tube that moves the sample

in the z-direction to maintain constant force, while shifting in the x- and y-directions in scanning the specimen. To eliminate some of the distortion effects of a piezoelectric tube scanner, however, three separate piezo crystals may also be used with each responsible for scanning for each of the orthonormal x-, y-, and z-directions. The piezoelectric materials expand and contract proportionally to an applied voltage, where elongation or contraction is induced by the polarity of the applied voltage, due to its ability to generate electric potential in response to applied mechanical stress.

Depending on the application, AFM is operated in different modes, generally divided between static/contact and dynamic/non-contact modes. In contact mode, constant deflection of the cantilever is maintained during scanning to keep the force between the probe tip and sample surface constant. In non-contact modes, a small piezoelectric element mounted in the AFM tip holder externally oscillates the probing cantilever at or close to its fundamental resonance frequency or a resonance harmonic to detect tip-sample interaction forces via changes in oscillation amplitude, phase, and resonance frequency with respect to the external reference oscillation. Information is acquired in non-contact modes by either frequency or amplitude modulation, through either changes in oscillation frequencies or oscillation amplitude or phase, respectively. Here, a feedback loop system adjusts the average tip-to-sample separation distance to maintain constant oscillation amplitude or frequency. Oscillation amplitude or frequency decreases as the tip is brought closer to the sample due to Van der Waals forces, which are strongest between 1 to 10 nm above the surface. The topographic image of the sample surface is then generated by tip-to-sample distance data at each (x, y) data point on the two-dimensional surface.

To keep probe tips close enough to samples for detection of short-range interactive forces while preventing tips from sticking to a liquid meniscus layer that develops on sample surfaces in ambient atmospheres, dynamic contact mode or tapping mode could also be used, where distance between cantilever tip and sample surface is modulated as the cantilever is oscillated at greater than 10 nm, typically from 100 to 200 nm.[22] In the tapping mode, an electric servo connected to a piezoelectric actuator controls separation distance between cantilever and sample to maintain at set cantilever oscillation amplitude while scanning. By imaging the force of oscillating contacts of the probe tip with the sample surface rather than probing the cantilever across the sample surface at constant force, the tapping mode is gentler than the contact mode, resulting in less surface damage, which is especially important for soft samples such as organic and polymeric thin films.

Sessile Drop Technique

The contact angle, defined as the angle made by the intersection of the liquid/solid and the liquid/air interfaces, of a probe liquid of known surface energy on a perfectly flat, solid surface directly provides information about the interaction energy between the surface and the liquid via the following Young Relation (**Equation 1.5**) that states that at equilibrium the chemical potentials of the liquid phase of the droplet, the solid phase of the substrate, and the gas/vapor phase of ambient atmosphere, which also includes an equilibrium concentration of the liquid vapor, must be equal:[23]

$$\gamma_{SV} - \gamma_{SL} - \gamma \cos\theta_C = 0 \quad \textbf{(Equation 1.5)}$$

where γ_{SV} = solid/vapor interfacial energy (surface energy of solid), γ_{SL} = solid/liquid interfacial energy, γ = liquid/vapor interfacial energy (surface tension of liquid), and θ_C = equilibrium contact angle (for $0° < \theta_C < 180°$)

According to the Young Relation, equilibrium contact angle and surface energy of the solid substrate are inversely related. In the static sessile drop method used for monitoring substrate surface energies in this experiment, a contact angle goniometer is used with a high-resolution CCD camera to capture images of water droplets on substrates after deposition via a syringe pointed vertically down onto the sample surface from a fixed position on top of the goniometer. Image analysis software is then used to measure the angle formed between the liquid/solid and liquid/vapor interfaces. With large enough sample surfaces, multiple droplets are deposited in various locations on the sample to determine the heterogeneity of the specimen's surface energy properties.

Objectives of Research

In this work, procedures were developed for growing surface-bound Nb and furan-maleic anhydride (FMA) homopolymers, as well as Nb-FMA and FMA-Nb block copolymers on silicon-oxide/silicon (SiO_x/Si) substrates via surface-initiated ring-opening metathesis polymerization (SI-ROMP) from 7-octenyltrichlorosilane (7-OCT) monolayers with First Generation Grubbs Catalyst, which were monitored by ellipsometry. Besides chemical functionalization of monomer, functionality was also introduced into polymer brushes via end-functionalization of grafted polymer chain-ends as another technique of altering surface energy and wettability. As a proof of concept, end-functionalization of surface-bound polymer brushes through cross-metathesis reactions with vinyl containing compounds styrene and 4-vinylpyridine were demonstrated and confirmed by static contact angle measurements of water droplets.

CHAPTER 2
EXPERIMENTAL

Cleaning Silicon Wafers

Silicon wafers (Silicon quest) with native oxide were cut into 0.5 x 2.0 cm^2 plates and placed in a slide holder. Enough 10:1 (water : ultrasonic cleaning solution) (Fisherbrand®) dilute ultrasonic cleaning solution was poured into the slide holder to cover the silicon wafers. Silicon wafers in the slide holder with dilute ultrasonic cleaning solution were sonicated for 5 min to remove hydrophobic contaminants. The slide holder was decanted. The slides were then sonicated with 18.2 MΩ purified, deionized water for 5 min. 5-min sonications were repeated in acetone, isopropanol, and purified deionized water. Silicon wafers were blown dry with nitrogen and oven-dried. Oven-dried silicon wafers were placed in an aluminum foil dish with the surface to be cleaned faced up. The silicon wafers in the aluminum foil dish were placed in a PSD-UV surface decontamination system (Novascan) for 20 minutes to remove residual hydrocarbon impurities, yielding hydrophilic surfaces.

7-Octenyltrichlorosilane (7-OCT) Monolayer Assembly

A 0.5 x 2.0 cm^2 plate of glass was placed on the bottom of a desiccator. Cleaned silicon wafers were placed on a metal grid above the glass plate. Five drops of 7-octenyltrichlorosilane (7-OCT) (Gelest) were applied on top of the glass slide on the bottom of the desiccator. 7-OCT was then vaporized by reducing the pressure in the desiccator to approximately 500 torr under continuous vacuum for 5 minutes and then static vacuum for 25 minutes at room temperature. Silicon slides were sonicated in acetone for 5 minutes to dislodge physisorbed material.

Ellipsometric measurements were made on 7-OCT monolayer to confirm a thickness of 13-15 Å, corresponding to full, uniform coverage of 7-OCT on the surface. Atomic force microscope (AFM) images of monolayers were also taken to confirm their completeness and uniformity.

Furan-Maleic Anhydride (FMA) Monomer Synthesis

5.98 g of maleic anhydride and 4.10 g of furan (stoichiometric ratio of 1:1) was added to 100 mL of diethyl ether in a 500-mL round-bottom flask and stirred at room temperature for 24 hours under nitrogen atmosphere. White precipitate was vacuum filtered and excess furan was distilled under reduced pressure at room temperature to obtain the desired product. Yield: 5.50 g (55.0%). ^{1}H NMR (δ ppm, in DMSO) 6.58 (s, 2H), 5.35 (s, 2H), 3.31 (s, 2H) (See *Appendix A* for ^{1}H NMR spectrum).

Surface-Initiated Ring-Opening Metathesis Polymerization (SI-ROMP)

All surface-initiated ring-opening metathesis polymerization (SI-ROMP) procedures except for polymerization of FMA were conducted in an air-free, nitrogen glove box (MBraun Unilab). Four silicon wafers with 7-OCT monolayers were immersed in 10 mM First Generation Grubbs Catalyst (Aldrich) solution of anhydrous, degassed dichloromethane (DCM) for 30 min to activate substrates for ring-opening metathesis polymerization (ROMP). Solvents were degassed by bubbling argon gas in them for 30 minutes. Silicon substrates were quickly dipped once into a beaker with 30 mL anhydrous, degassed DCM to rinse off excess, unattached Grubbs Catalyst. To make surface-tethered norbornene (Nb) homopolymers, two Grubbs-activated silicon substrates were placed in 0.056 M Nb monomer solution of anhydrous, degassed DCM for 30 minutes. To make surface-tethered FMA homopolymers, the other two Grubbs-activated silicon substrates were placed in 0.5 M FMA monomer solution of anhydrous, degassed tetrahydrofuran (THF) and sealed under nitrogen gas in the glove box. Then the sealed container

with the two substrates in FMA monomer solution was transported out of the glove box and placed in an oil bath for 30 minutes at 50 °C. To make surface-tethered Nb-FMA block copolymers, one of the two Grubbs-activated silicon substrates that were previously reacted in 0.056 M Nb monomer solution were swiftly immersed in 0.5 M FMA monomer solution of anhydrous, degassed THF and sealed under nitrogen gas in the glove box. Then the sealed container with the substrate in FMA monomer solution was transported out of the glove box and placed in an oil bath for 30 minutes at 50 °C. To make surface-tethered FMA-Nb block copolymers, one of the two Grubbs-activated silicon substrates that were first reacted in 0.5 M FMA monomer solution were swiftly immersed in 0.056 M Nb monomer solution of anhydrous, degassed DCM for 30 minutes. Polymerizations were terminated by the addition of several drops of ethyl vinyl ether. All substrates with surface-tethered polymer brushes were sonicated in acetone to remove excess physisorbed material. Polymerizations were monitored by taking ellipsometric measurements of polymer thickness. Synthetic procedures are outlined in **Figures 2.1-2.2**.

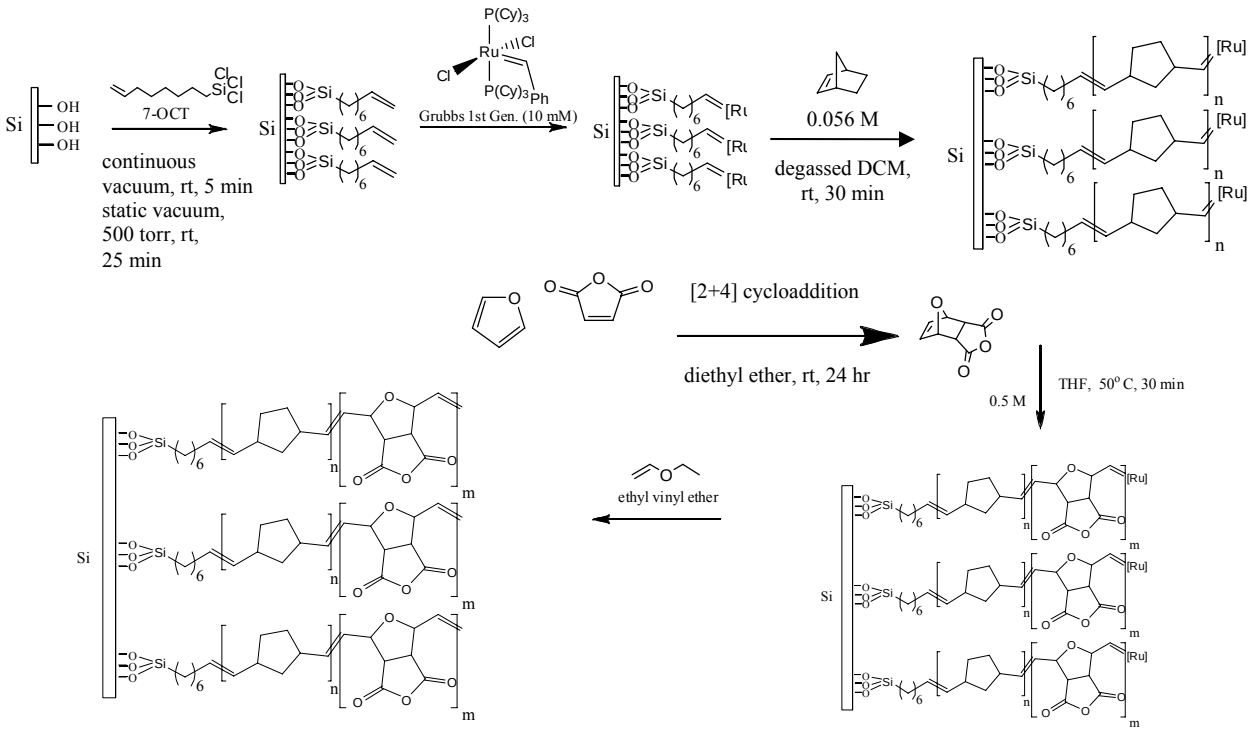

Figure 2.1: Monomer Synthesis and Polymerization Scheme for Growing Surface-Initiated Norbornene-Furan/Maleic Anhydride (SI-Nb-FMA) Block Copolymer Brushes on Silicon Oxide/Silicon (SiO_x/Si) Surface.

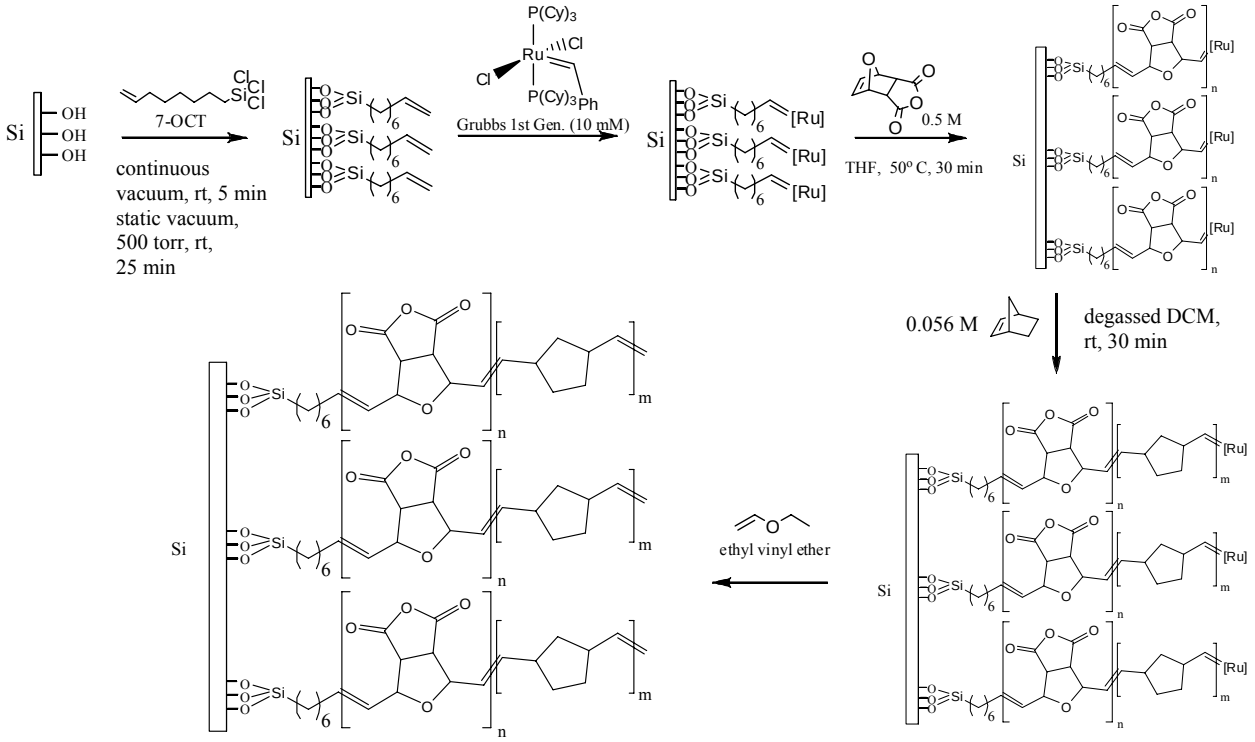

Figure 2.2: Polymerization Scheme for Growing Surface-Initiated Furan/Maleic Anhydride-Norbornene (SI-FMA-Nb) Block Copolymer Brushes on SiO_x/Si Surface.

End-Functionalization

Substrates with surface-tethered Nb polymer brushes were immersed in solutions of the desired vinyl containing compound for end-functionalization without quenching in ethyl vinyl ether solution. To end-functionalize with styrene, substrates were immersed in 10 mM styrene solution in anhydrous, degassed DCM. To end-functionalize with 4-vinylpyridine, substrates were immersed in 10 mM 4-vinylpyridine solution in anhydrous, degassed DCM. The 4-vinylpyridine brushes were protonated in 0.1 M hydrochloric acid (HCl) solution of 18.2-MΩ purified, deionized water.

Ellipsometric Characterizations

Thickness data for monolayers and polymer films were determined as the mean value of ellipsometric measurements at three random places on the substrate. Null ellipsometry was performed on a Multiskop (Optrel, GbR) with a 632.8 nm He-Ne laser beam as the light source. An integrated, specialized software calculated thickness from measured values for Δ and Ψ.

Atomic Force Microscope (AFM) Characterizations

Surface morphologies of selected substrates were characterized by AFM. AFM experiments were performed using Multimode Nanoscope IIIa (Digital Instruments/Vecco Metrology Group) in the tapping mode.

Contact Angle Characterization

Static contact angle measurements of water droplets were made on end-functionalized substrates after quaternization using the Multiskop (Optrel, GbR). The contour of a water droplet was analyzed and fitted to the Young-Laplace equation using a contour tracing algorithm. The contour image was detected with a CCD camera using a white light source. The contact angle measurement of a substrate was determined as the mean value of contact angle measurements at

three random places on the substrate. Statistical uncertainties were calculated as the standard deviation of contact angle measurements at three random places on each substrate.

CHAPTER 3
RESULTS AND DISCUSSION

Presently, synthesis and characterization of polymer brushes have grown tremendously in sophistication.[24] The "grating-from" approach in growing functional surface-bound polymer brushes has proven to be effective in greatly enhancing the number of large polymer chains covalently attached to the surface. Furthermore, chemical functionalization of monomers greatly enhances the density of functional groups in a limited surface area by presenting functionality in each monomer repeat unit.[25] By coupling the "grating-from" approach using living polymerization techniques such as surface-initiated ring-opening metathesis polymerization (SI-ROMP) with chemical functionalities of different monomer architectures, chemical and physical characteristics derived from various chemical functionalizations are amplified.

Specifically, it has been possible to grow norbornene (Nb) and furan-maleic anhydride (FMA) homopolymers, as well as Nb-FMA and FMA-Nb block copolymers from silicon oxide/silicon (SiO_x/Si) surfaces from 7-octenyltrichlorosilane (7-OCT) monolayers via SI-ROMP with First Generation Grubbs Catalyst. Polymerizations were only effective on uniform 7-OCT monolayers, whose smoothness and closed-packed morphologies were confirmed via atomic force microscopy (AFM) (**Figure 3.1**). **Table 3.1** shows growth of these polymers as monitored via ellipsometry. A mean thickness value was determined by averaging ellipsometric data at three different places on the substrate and statistical uncertainty was determined as the standard deviation of the three data points. AFM images of the various homopolymers and block copolymers confirm the synthesis of uniform, smooth polymer films with slightly varying

morphologies due to their different chemical and physical characteristics (**Figures 3.2-3.4**). As the globular morphology observed by AFM suggests, polymer chains are packed closely next to each other at relatively high densities. Apart from the large circular defects observed in the FMA polymer brush substrates, possibly due to physisorbed polymer generated by chain transfer of initiator from the surface, the consistency of polymer brush morphological patterns throughout scan ranges confirm the synthesis of uniform surface-tethered homopolymer and block copolymer brushes.

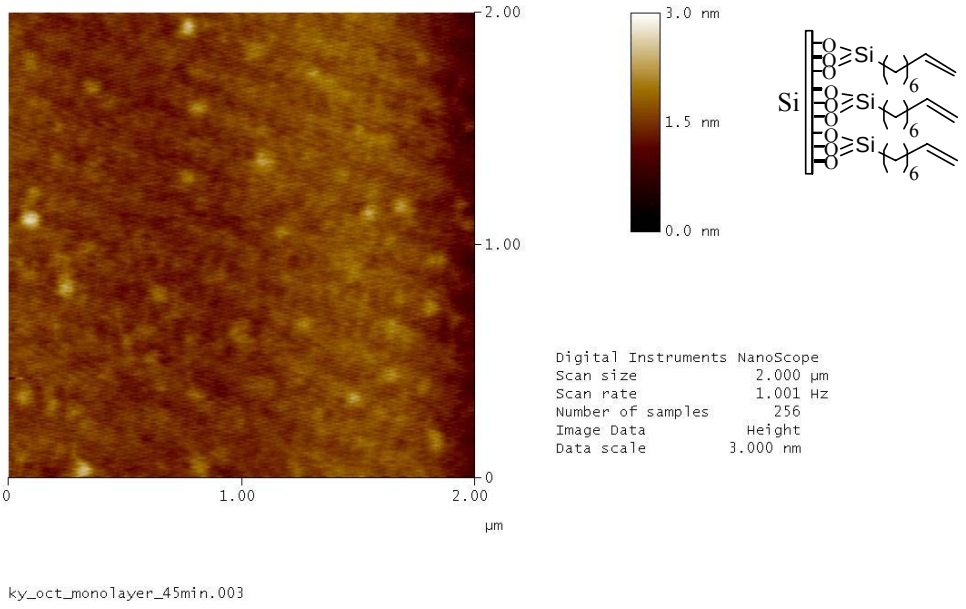

Figure 3.1: Atomic Force Microscope (AFM) Image of 7-Octenyltrichlorosilane (7-OCT) Monolayer on Silicon Oxide/Silicon (SiO_x/Si) Surface.

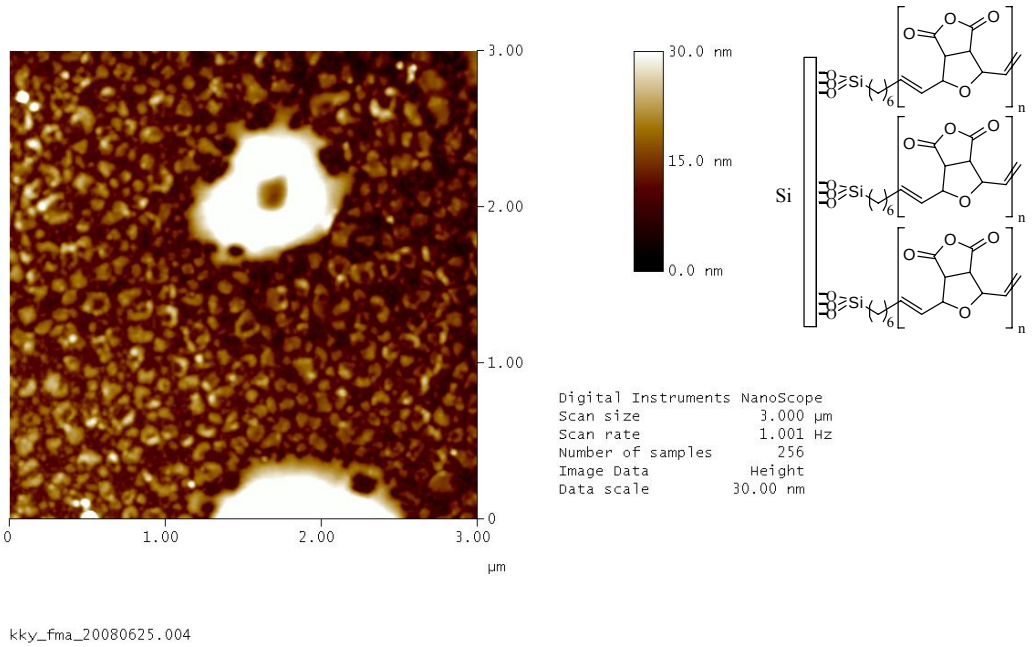

Figure 3.2: AFM Image of Surface-Initiated Furan-Maleic Anhydride (SI-FMA) Homopolymer Brushes on SiO_x/Si Surface.

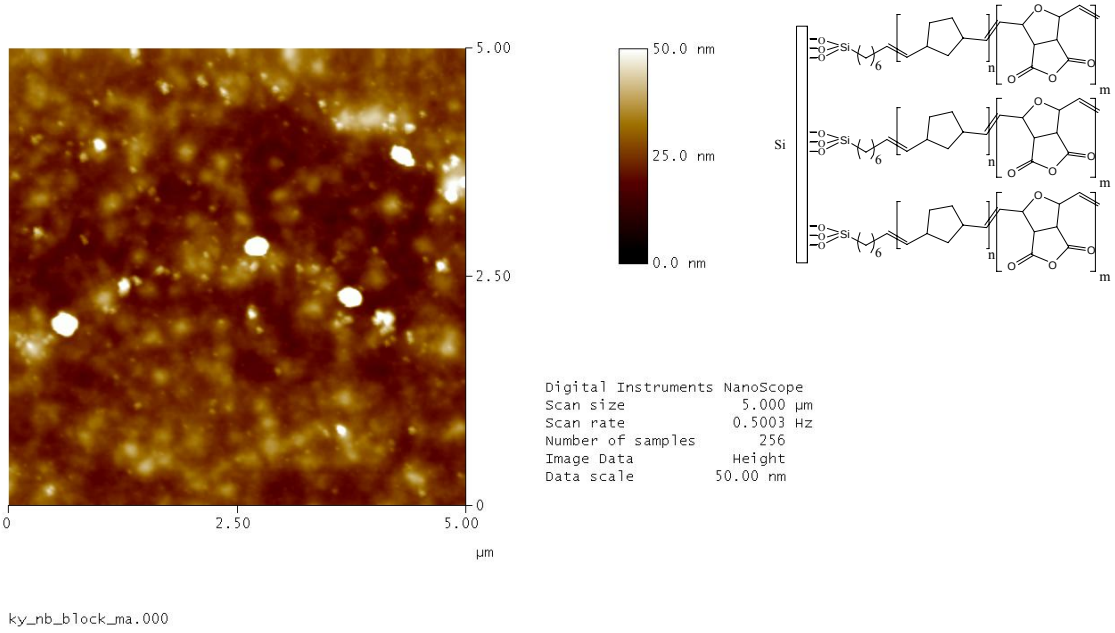

Figure 3.3: AFM Image of Surface-Initiated Norbornene-Furan/Maleic Anhydride (SI-Nb-FMA) Block Copolymer Brushes on SiO_x/Si Surface.

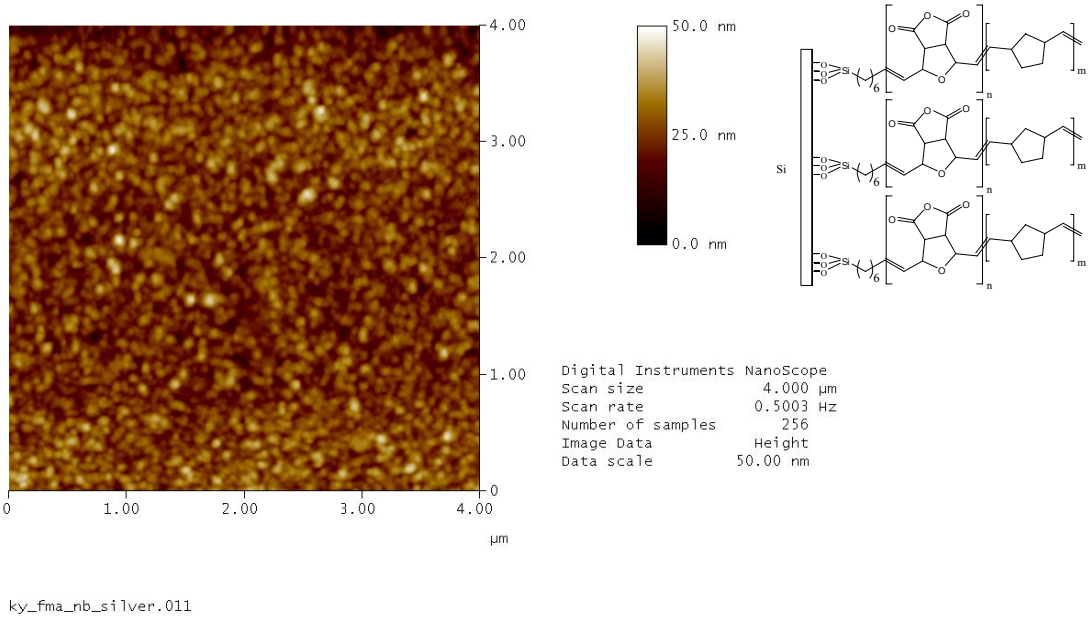

Figure 3.4: AFM Image of Surface-Initiated Furan/Maleic Anhydride-Norbornene (SI-FMA-Nb) Block Copolymer Brushes on SiO_x/Si Surface.

Table 3.1: Ellipsometric Characterization of Brush Thickness of Homopolymers and Block Copolymers. 7-OCT=7-octenyltrichlorosilane; FMA=furan-maleic anhydride; Nb=norbornene.

Film	*Thickness (nm)*	*Average Thickness (nm)*
7-OCT Monolayer	3.05	**2.60 ± 0.34**
	2.53	
	2.41	
FMA Polymer Brush	21.28	**22.00 ± 2.52**
	24.69	
	19.76	
FMA-Nb Polymer Brush	33.25	**35.50 ± 1.97**
	37.06	
	36.04	
Nb Polymer Brush	6.82	**7.12 ± 0.28**
	7.16	
	7.37	
Nb-FMA Polymer Brush	46.10	**44.90 ± 2.13**
	42.45	
	46.17	

By carefully and rapidly transferring substrates that contain growing polymer chain-ends from one monomer solution to another, it was possible to maintain catalyst activity and produce surface-tethered block copolymers via ROMP. Verification of the creation of surface-tethered block copolymers was possible through careful experimental design. Since film thicknesses increased upon polymerization in second monomer solutions, surface-tethered block copolymers were indeed synthesized successfully (**Table 3.1**).

Differences in film growth for varying experimental conditions between Nb and FMA polymerization via ROMP reveal effects of monomer properties and concentrations and reaction temperature on polymerization kinetics. To form polymer brushes within the detection limits of ellipsometry, reaction conditions for the growth of Nb and FMA polymer layers were optimized to maintain equal and controllable thickness values. Since Nb polymerized more readily than FMA, it was reacted from concentrations lower than those of FMA by almost one order of magnitude—0.056 M for Nb and 0.5 M for FMA. However, even at higher concentrations of 0.5 M, FMA could not still polymerize appreciably at room temperature, requiring the reaction temperature to be raised to 50 °C. Although Grubbs Catalysts tolerate more functional groups on monomers for initiating ROMP than other olefin metathesis catalysts, it is known that substituents on cyclic monomers, including the oxygen heterocycle and carboxylic acid groups of FMA, could still interact with the catalyst to decrease its reactivity, which occurs in the case of FMA with First Generation Grubbs Catalyst.[26] Tetrahydrofuran (THF), the only available solvent that could sufficiently dissolve FMA at higher temperatures, could not dissolve FMA at higher concentrations than 0.5 M. Polymer brush thickness data show that for the same reaction times, FMA homopolymer brushes grew thicker than Nb homopolymer brushes by 14.88 nm and that the FMA layer in Nb-FMA block copolymer brushes grew also to greater thickness than the

Nb layer in FMA-Nb block copolymer brushes by 24.28 nm. Hence, it was possible to polymerize FMA at higher rates than Nb after increasing its concentration nearly ten-fold and raising the reaction temperature from room temperature to 50 °C, although FMA is inherently less prone to polymerization than Nb.

Along with introducing chemical functionalities within each repeating monomer—such as the carboxylic moieties in FMA that can be brought about through hydrolysis of the anhydride functionality—it was also possible to functionalize the ends of growing surface-bound polymer chains through cross-metathesis reactions. End-functionalization of norbornene homopolymer brushes grown via SI-ROMP with styrene and 4-vinylpyridine were confirmed by static contact angle measurements as shown in **Table 3.2**. SiO_x/Si surfaces before surface-initiated polymerization were highly oxidized and characterized with high surface energies. Since Nb polymers are hydrophobic relative to the SiO_x/Si metallic surface, surface energy of the SiO_x/Si substrate decreases with increasing Nb polymer brush thickness. However, for thicknesses above at least approximately 13 nm, Nb brush thickness ceased to make a difference on the surface energy of the SiO_x/Si substrate. Beyond at least 13 nm, there was complete surface coverage and high chain density of Nb polymer brushes at the SiO_x/Si surface, resulting in surface energies influenced solely by the Nb polymer brushes. Although Nb polymer brush thicknesses increased by 7 nm for styrene-end-functionalized Nb polymer films and by 24 nm for 4-vinylpyridine-end-funcionalized Nb polymer films from Trial 1 to Trial 2, there was no significant change in static contact angle measurements between the two trials for each type of end-functionalization. Therefore, differences in contact angle of about 10 degrees between styrene- and 4-vinylpyridine-end-functionalized Nb polymer films could be attributed solely to the end-functionalizations

Table 3.2: Effect of End-Functionalization on Surface Energy After Acid Treatment.

Styrene End-Functionalization			
Trial 1			
Nb Brush Thickness (nm)	*Average (nm)*	*Contact Angle (degrees)*	*Average (degrees)*
20.79	**20.39 ± 0.54**	92.9	**92.5 ± 0.5**
19.77		91.9	
20.61		92.7	
Trial 2			
Nb Brush Thickness (nm)	*Average (nm)*	*Contact Angle (degrees)*	*Average (degrees)*
31.44	**27.68 ± 3.48**	91.1	**91.3 ± 0.4**
27.04		91.8	
24.56		91.1	
4-Vinylpyridine End-Functionalization			
Trial 1			
Nb Brush Thickness (nm)	*Average (nm)*	*Contact Angle (degrees)*	*Average (degrees)*
13.36	**13.26 ± 0.97**	82.9	**82.5 ± 1.8**
14.18		80.5	
12.24		84.1	
Trial 2			
Nb Brush Thickness (nm)	*Average (nm)*	*Contact Angle (degrees)*	*Average (degrees)*
34.21	**37.27 ± 9.90**	81.4	**82.6 ± 1.3**
48.34		83.9	
29.26		82.6	

Water droplet contact angle measurements on 4-vinylpyridine-end-functionalized Nb polymer films were lower by 10 degrees than those on styrene-end-functionalized Nb polymer films because after protonation using dilute hydrochloric acid (HCl), the 4-vinylpyridine end-functionality was protonated with higher surface energy while the styrene end-functionality remained unaffected, retaining its nonpolarity and low surface energy (**Figures 3.5-3.6**). Thus, by simply immersing Grubbs-activated surface-bound polymer brushes into solution with a vinyl compound it was possible to end-functionalize polymer brushes via cross-metathesis. Other than careful synthetic design of new monomers, this technique of end-functionalization provides

another option of introducing chemical functionality at the surface but at a much lower concentration.

Figure 3.5: Water Droplets on Styrene End-functionalized Norbornene (Nb) Polymer Brush Surface After Acid Treatment.

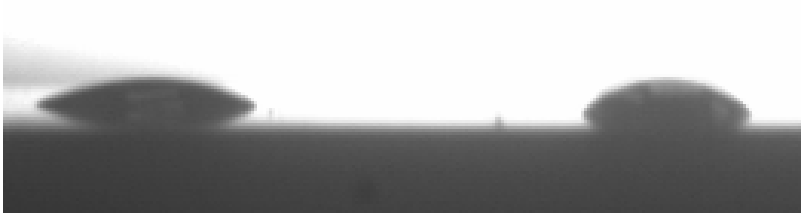

Figure 3.6: Water Droplets on 4-Vinylpyridine End-functionalized Nb Polymer Brush Surface After Acid Treatment.

Conclusion and Future Work

By using SI-ROMP with First Generation Grubbs Catalyst, Nb and FMA homopolymer brushes, as well as Nb-FMA and FMA-Nb block copolymer brushes were grown from SiO_x/Si surfaces from 7-OCT monolayers. Monomer structure and concentration, as well as reaction time and temperature all affected the surface-initiated polymerization mechanism. End-functionalization of Grubbs-activated surface-bound polymer brushes with vinyl compounds were performed and verified by static water contact angle measurements.

While this thesis reports procedures for synthesizing homopolymer brushes and block copolymer brushes with layers characterized by greatly differing chemical characteristics, such as polarity and solubility in water, its work needs to be extended to investigations of the physical and chemical characteristics of these brushes. AFM investigations of solvent-induced changes in block copolymer brush morphologies could reveal reorganization of block copolymer brushes as its layers interact differently to solvents of varying polarities. Solvent-induced changes in contact angle of surfaces with block copolymer brushes may also be detectable for optimized thicknesses of hydrophilic and hydrophobic layers in block copolymer chains.

While polymer brushes have been primarily synthesized on flat surfaces with modifications in surface properties invoked by chemical properties of the polymer, synthesis on patterned or rough surfaces could also potentially alter surface properties. Various patterning techniques are available for fabricating patterned polymer brushes, including microcontact printing (μCP), UV/electron-beam lithography, scanning-probe lithography, and imprint lithography.[27] Combining capillary force lithography (CFL) and surface-initiated polymerization has also been proven effective in synthesizing patterned binary polymer brushes.[6] Combining sophisticated techniques for both polymer brush synthesis and surface-patterning would create highly functional surfaces, which would ultimately allow conception and development of novel materials and devices of biomedical, technological, and electronic interest, which take advantage of the properties inherent in thin polymer films.

APPENDIX A

^{1}H NMR SPECTRUM OF FURAN-MALEIC ANHYDRIDE (FMA) MONOMER

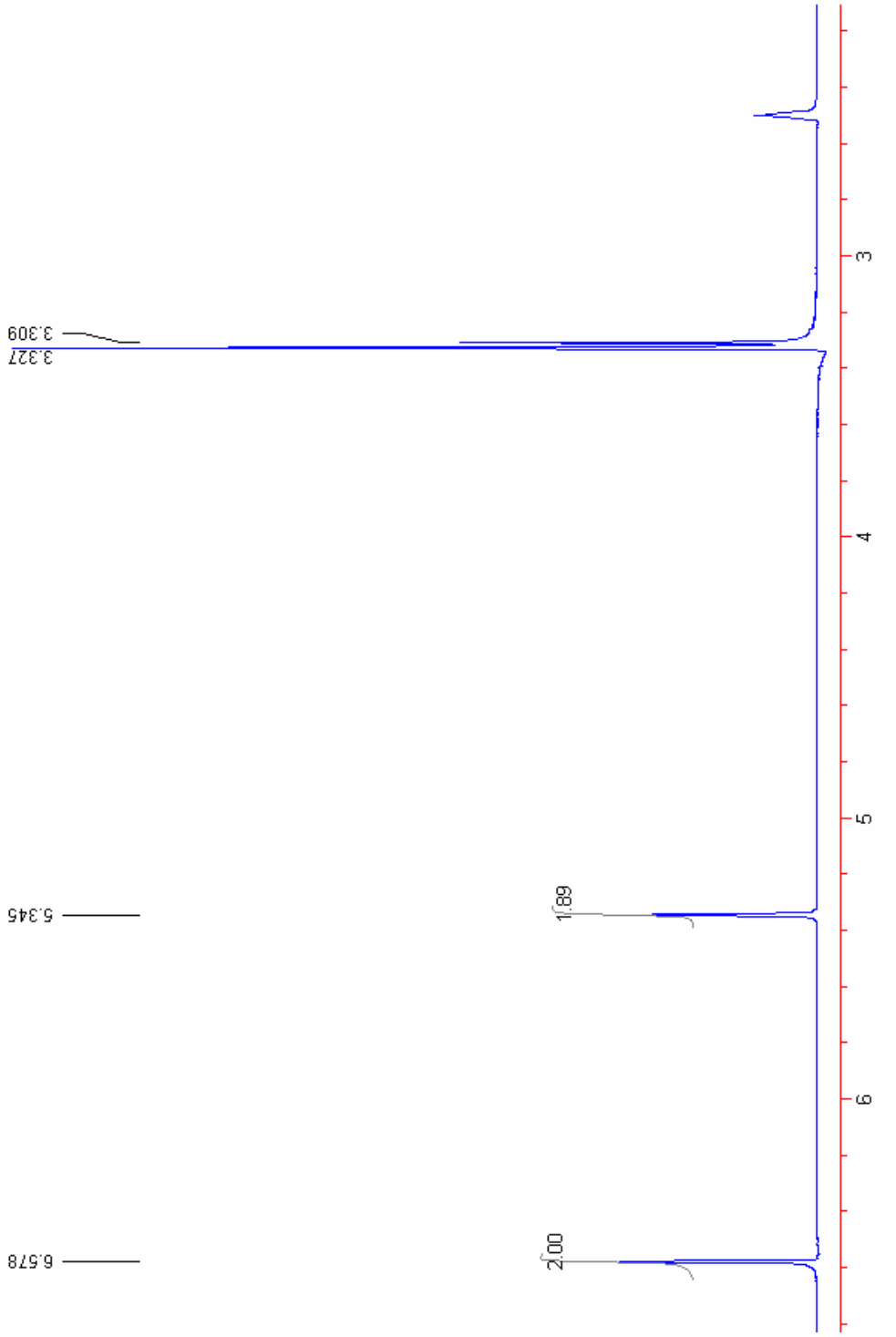

WORKS CITED

1. Zhao, B; Moore, J. S.; Beebe, D. J. *Science*, **2001**, *291*, 1023-1026.

2. A La Van, D.; McGuire, T.; Langer, R. *Nat. Biotechnol.*, **2003**, *21*, 1184–1191.

3. Ikeda, T.; Tsutsumi, O. *Science*, **1995**, *268*, 1873–1875.

4. Kawata, S.; Kawata, Y. *Chem. Re*v., **2000**, *100*, 1777–1788.

5. Hugel, T.; Holland, N. B.; Cattani, A.; Moroder, L.; Seitz, M.; Gaub, H. E. *Science*, **2002**, *296*, 1103–1106.

6. Pace, G.; Ferri, V.; Grave, C.; Elbing, M.; von Hanisch, C.; Zharnikov, M.; Mayor, M.; Rampi, M. A.; Samori, P. *Proc. Nat. Acad. Sci. U.S.A.*, **2007**, *104*, 9937–9942.

7. Yang, D.; Piech, M.; Bell, N. S.; Gust, D.; Vail, S.; Garcia, A. A.; Schneider, J.; Park, C. D.; Hayes, M. A.; Picraux, S. T. *Langmuir*, **2007**, *23*, 10864–10872.

8. Oh, S.-K.; Nakagawa, M.; Ichimura, K. *J. Mater. Chem.*, **2002**, *12*, 2262–2269.

9. Blossey, R. *Nat. Mater.*, **2003**, *2*, 301–306.

10. Fries, K.; Samanta, S.; Orski, S.; Locklin, J. *Chem. Comm.*, **2008**, 6288.

11. Schwartz, D.K. *Annu. Rev. Phys. Chem.,* **2001**, *52*, 107.

12. Wnek, G.; Bowlin, G. L., Ed. *Encyclopedia of Biomaterials and Biomedical Engineering*, 2nd ed. 1st vol. New York: Informa Healthcare USA, Inc., 2004, 1331-1333.

13. Love, J. C.; Estroff, L. A.; Kriebel, J. K.; Nuzzo, R. G.; Whitesides, G. M. *Chem. Rev.*, **2005**, *105*, 1103-1169.

14. Hérisson, J. L.; Chauvin, Y. *Makromol. Chem.*, **1971**, *141*, 161.

15. Soufflet, J. P.; Commereuc, D.; Chauvin, Y.; Hebd, C. R. *Seances Acad. Sci. Série C*, **1973**, *276(2)*, 169.

16. Dragutan, I.; Dragutan, V.; Filip, P. *ARKIVOC*, **2005**, *5*, 105-129.

17. Grubbs, R. H., Ed. *Handbook of Metathesis*, 1st vol. New York: Wiley-VCH, 2003**.**

18. Hejl, A.; Scherman, O. A.; Grubbs, R. H. *Macromolecules*, **2005**, *38(17)*, 7214–7218.

19. Mol, J. C. *J. Mol. Catal.,* **2004**. *213 (1)*, 39-45.

20. Fu, G. C.; Nguyen, S. T.; Grubbs, R. H. *J. Am. Chem. Soc.*, **1993**, *115*, 9856.

21. Hinterdorfer, P.; Dufrêne, Y. F. *Nat. Meth.*, **2006**, *3*, 5.

22. Zhong, Q.; Inniss, D.; Kjoller, K.; Elings, V. B. *Surf. Sci. Lett.*, **1993**, *290*, L688.

23. Young, T. *Phil. Trans. R. Soc. Lond.*, **1805**, *95*, 65-87.

24. Ulman, A. *Chem. Rev.* **1996**, *96(4)*, 1533-1539.

25. Advincula, R. C.; Brittain, W. J.; Baster, K. C.; Ruhe, *J. Polymer Brushes: Synthesis, Characterization, Applications,* **2004**.

26. Slugovc, C.; Demel, S.; Riegler, S.; Hobisch, J.; Stelzer, F. *J. Mol. Catal.*, **2004**, *213(1)*, 107-113.

27. Liu, Y.; Klep, V.; Luzinov, I. *J. Am. Chem. Soc.*, **2006**, *128(25),* 8106-8107